Int J Adv Manuf Technol (2006) 29: 648–654
DOI 10.1007/s00170-005-2573-5

ORIGINAL ARTICLE

C.-K. Chen · Y.-M. Tsao

A stability analysis of regenerative chatter in turning process without using tailstock

Received: 2 August 2004 / Accepted: 18 January 2005 / Published online: 24 March 2006

Abstract A new approach to analyze the stability of cutting processes when considering the deformation of the workpiece is proposed in this article. In past studies, the workpiece was assumed to be rigid and no deformation was considered. In those studies, the stability of the cutting process was analyzed by merely the dynamic equation of tools. However, the workpiece does have deformation when there is external force exerting on it. Such deformation will change the chip thickness and have an effect on the critical chip thickness of stability. To describe the cutting in turning process, partial differential equations are used and a set of dynamic equations will be considered based on the interaction between the tool and the workpiece. After performing the Laplace transformation, stability can be analyzed based on the length, radius, natural frequency, deflection, aspect ratio and material stiffness of the workpieces. The effect of the critical chip width under different spindle speed will also be discussed in this article. By considering the deformation of the workpiece under different conditions, the results show that the critical chip width of the deformed case is always larger than the rigid body case.

Keywords Chatter · Turning · Regenerative · Stability

1 Introduction

Turning is a single-point machining process which is used in machine castings, forgings and in other components which require precision dimensional tolerance and good surface finish. In order to increase the cutting speed, the chip thickness and chip width are often increased, which will result in forced vibration and an extremely large cutting force at the contact point. The result of violent chatter causes numerous adverse effects, such as lowering the life span of tools, inaccurate dimensions, low surface quality, unacceptable noise and tool damage.

The vibration in the cutting process is a dynamically unstable phenomenon [1, 2] which has been studied for a long time. Dynamics, structural and limiting stability have been studied in the past [1, 3], where mathematical models considered the direct cutting behavior in common. Other studies have focused on the choice of controlling parameters in order to avoid unexpected vibrations [4–9]. In addition, some researchers have established the fundamental principle of vibration phenomena. However, the vibration cannot be observed in real-time, and the control to compensate the vibration cannot be made either [10–16].

Regenerative and non-regenerative chatters are two kinds of machine tool chatter that are widely accepted in modern research. Regenerative chatter results from cutting on the previous surface of waves; and non-regenerative chatter occurs in some special circumstances, as described in [6]. In the past studies, the workpiece was assumed to be rigid, and only the tool vibration was considered. However, since the tool will exert force on the workpiece, there will be workpiece deflection and the chip thickness will be changed. Therefore, they have a great effect on the cutting behavior.

In this article, we focus on the regenerative chatter where a flexible workpiece is considered rather than a rigid assumption. To fully describe the vibration behavior, two models are used for the workpiece and the tool, which correspond to a second order partial differential equation and a second order ordinary differential equation, respectively. The interaction between the workpiece and the tool can be discussed and analyzed based on these models. This article is organized as follows: the introduction of cutting models is presented in Sect. 2, a stability analysis is presented in Sect. 3, simulation results and discussions are offered in Sect. 4, and in Sect. 5 we offer our conclusions.

2 Dynamic cutting model

The dynamic cutting model will be discussed into two parts: first, the deflection of the tool will not be taken into consideration; sec-

C.-K. Chen
Department of Mechanical Engineering,
National Cheng Kung University, Tainan, Taiwan, R.O.C.
E-mail: ckchen@mail.ncku.edu.tw

Y.-M. Tsao
Departmenzt of Automation and Control Engineering,
Far East College, Tainan, Taiwan, R.O.C.

ond, the deflection produced by the tool force will be considered, hence the effect of the deflection on the stability can be included.

To clearly formulate the problem, a simplified cutting system is adopted and only one dimensional second order dynamic orthogonal cutting model, as shown in Fig. 1, is used in the analysis. In the process of orthogonal cutting, considering the end point cutting of the workpiece, the chip overlapping factor, μ, is taken as 1, and the governing equation [17, 18] is represented by:

$$m\ddot{y}(t) + c\dot{y}(t) + ky(t) = F(t)\cos\theta. \tag{1}$$

where $y(t)$ is the offset chip thickness, which represents the fluctuation of the depth of cut at the time t; m is the equivalent mass of the tool system; c and k are the equivalent damping and stiffness, respectively; θ is a fixed cutting angle; and F is the cutting force. The cutting force is taken to be proportional to the chip area $bh(t)$ with a coefficient C being the proportional constant and can be written as follows:

$$F(t) = Cbh(t). \tag{2}$$

After the cutting process, the surfaces of the workpiece are all in the shape of waves, as shown in Fig. 1a, where $y(t-T)$ is the previous offset chip thickness of a cycle; h_0 is the nominal chip thickness resulting from the feed mechanism; T is the period of successive passages of the tool; and $y(t) - y(t-T)$ represents the produced regenerative character.

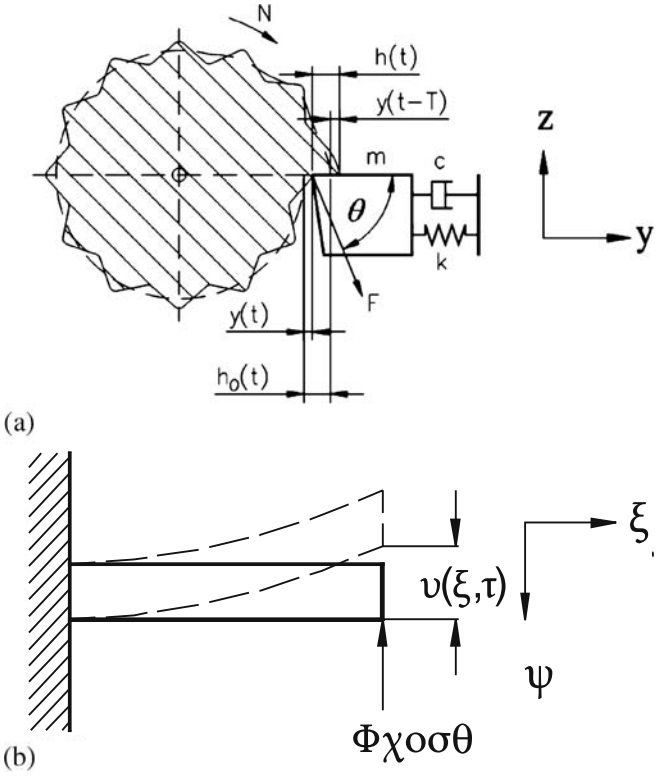

Fig. 1a,b. Orthogonal cutting diagram **a** Orthogonal cutting diagram considering a rigid-body workpiece **b** Deflection of workpiece considering deflection

Part I: Rigid workpiece. From Fig. 1a, the instant chip thickness can be written as follows:

$$h(t) = h_0 - y(t) + y(t-T). \tag{3}$$

Combining Eqs. 1–3 and performing the Laplace transformation we obtain the following:

$$\frac{Y(s)}{H_0(s)} = \frac{bCG(s)}{1 + bCG(s)(1 - e^{-Ts})}, \tag{4}$$

where $G(s) = \frac{\cos\theta}{ms^2+cs+k}$, and the block diagram of the system is shown in Fig. 2a.

Part II: Flexible workpiece. Consider a workpiece that is clamped at one side and free on the other side [1], just like the cantilever beam shown in Fig. 1b. When cutting is performed at the free end, the deflection of the workpiece will be generated due to the exerting force. Such deflection will affect both the real chip thickness and the cutting force, so Eq. 3 should be rewritten as:

$$h(t) = h_0 - y(t) + y(t-T) - u(x,t), \tag{5}$$

where $u(x,t)$ represents the workpiece deflection. Neglecting the torque and moment produced in the z-direction, the dynamic equation of the workpiece [19] now becomes

$$\frac{\partial^2}{\partial x^2}\left[EI\frac{\partial^2 u(x,t)}{\partial x^2}\right] + \rho A_c \frac{\partial^2 u(x,t)}{\partial t^2} = Cb\left[h_0 - y(t) + y(t-T) - u(x,t)\right]\delta(x-L)\cos\theta, \tag{6}$$

where E is the Young's modulus; I is the moment of inertia; ρ is the weight density; A_c is the cross section of a workpiece where these coefficients are fixed values; and $\delta(x-L)$ represents an impulse function. By means of the separation of variables, let

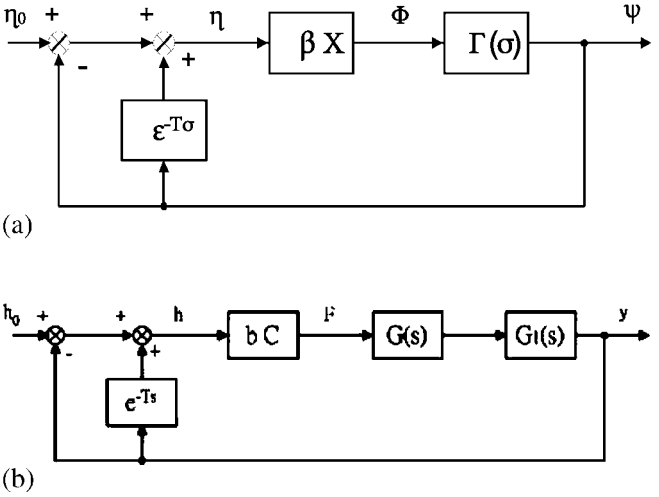

Fig. 2a,b. Block diagram of system **a** Block diagram of system considering a rigid workpiece **b** Block diagram of system considering deflection of the workpiece

$u(x,t)=\phi(x)q(t)$ and assume the boundary conditions are

$$u(0,t)=0,\ \left.\frac{\partial u(x,t)}{\partial x}\right|_{x=0}=0,\ \left.\frac{\partial^2 u(x,t)}{\partial x^2}\right|_{x=L}=0,$$
$$\left.\frac{\partial^3 u(x,t)}{\partial x^3}\right|_{x=L}=0,$$

the results can be obtained as

$$\phi_n(x)=A_n\left[\sin\alpha_n x-\sinh\alpha_n x+\frac{\sin\alpha_n L+\sinh\alpha_n L}{\cos\alpha_n L+\cosh\alpha_n L}(\cosh\alpha_n x-\cos\alpha_n x)\right], \quad (7)$$

$$\ddot{q}_n(t)+\omega_n^2 q_n(t)=\frac{1}{m_n}\int_0^L \phi_n(x)Cb\,[h_0-y(t)+y(t-T)-u(x,t)]\cos\theta\,\mathrm{d}x, \quad (8)$$

where $u(x)=\sum_{n=1}^{\infty}\phi_n(x)q_n(t)$, $m_n=\int_0^L \rho A_c\phi_n^2(x)\,\mathrm{d}x$,$\alpha_n L=\sqrt[4]{\frac{\omega_n^2\rho A_c L^4}{EI}}$ in Eq. 7 represents the characteristic value which is the solution of $1+\cos\alpha L\cosh\alpha L=0$, with ω_n representing the natural frequency of the workpiece. Since only the end point cutting is considered, therefore the equivalence "$x=L$" is assumed. When the natural frequency of the workpiece is much higher than the spindle speed, only the first mode dynamics is significant and will be taken into consideration. The results can be shown as follows:

$$\phi_1(L)=A_1\left[\sin\alpha_1 L-\sinh\alpha_1 L+\frac{\sin\alpha_1 L+\sinh\alpha_1 L}{\cos\alpha_1 L+\cosh\alpha_1 L}(\cosh\alpha_1 L-\cos\alpha_1 L)\right], \quad (9)$$

$$\ddot{q}_1(t)+\omega_1^2 q_1(t)=\frac{1}{m_1}\int_0^L \phi_1(x)Cb\times[h_0-y(t)+y(t-T)-\phi_1(x)q_1(t)]\,\delta(x-L)\cos\theta\,\mathrm{d}x, \quad (10)$$

Applying the Laplace transformation on Eqs 1 and 10, we get:

$$\frac{Y(s)}{H_0(s)}=\frac{bCG_1(s)G(s)}{1+bCG_1(s)G(s)(1-e^{-Ts})}, \quad (11)$$

where

$$G_1(s)=\frac{s^2+\omega_1^2}{s^2+\omega_1^2+Ab}$$
$$A=\frac{C\phi_1^2(L)\cos\theta}{\rho A_c\int_0^L\phi_1^2(x)\,\mathrm{d}x}.$$

In Eq. 11, $G(s)$ is the same as in Eq. 4 for the rigid workpiece case. The transfer function of the system can be treated as adding a pair of poles and a pair of zeros. Due to the relationship of $\omega_1^2<\omega_1^2+Ab$ in $G_1(s)$, those poles will be in the left hand side of zeros. From the stability analysis of a dynamic control system, it is apparent that this effect will increase the system stability. Considering H_0 as an input and Y as an output, the block diagram of the system is shown in Fig. 2b.

3 Stability analysis

Figure 2 shows the structure in equilibrium for this system when $y=0$. If the chip thickness is well distributed, then the vibration will not be generated and the cutting force F will remain unchanged. In addition, the deflection is kept fixed in the cutting process. When an impact occurs or a notch is passed, a small disturbance will exist, and the output will become small and close to zero. Such equilibrium is called "stable" or "asymptotically stable". The stability will be analyzed by the characteristic equation of the system. When considering the system stability, the I/O relationship of N and b will be discussed where N represents spindle speed (rev/s), and b represents chip width. In addition, N and b represent the parameters which can be controlled in turning process.

Part I: Rigid workpiece. Equation 4 is linear and its characteristic equation is:

$$1+bC\frac{\left(1-e^{-Ts}\right)\cos\theta}{ms^2+cs+k}=0, \quad (12)$$

let $s=j\omega$ and substitute into Eq. 12 and separate the real and the imaginary parts, the following critical parametric values [17] can be obtained:

$$b_1^*=\frac{(m\omega^2-k)^2+(c\omega)^2}{2C(m\omega^2-k)\cos\theta}, \quad (13a)$$

$$T_1^*=\frac{1}{\omega}\left\{(2n+1)\pi+a\tan\frac{2c\omega(m\omega^2-k)}{(m\omega^2-k)^2-(c\omega)^2}\right\}. \quad (13b)$$

From the above equation (assuming the spindle speed is fixed), it can be concluded that only the chip width is lower than b_1^*, and stable cutting can be obtained.

Part II: Flexible workpiece. Equation 11 is linear and its characteristic equation is as follows:

$$1+bC\frac{s^2+\omega_1^2}{s^2+\omega_1^2+Ab}\frac{(1-e^{-Ts})\cos\theta}{ms^2+cs+k}=0, \quad (14)$$

where ω_1 is the natural frequency of the workpiece in the first mode. Substituting $s=j\omega$ into Eq. 14 and separating the real and imaginary parts, the following critical parametric values will be obtained:

$$b_2^*=\frac{(m\omega^2-k)^2+(c\omega)^2}{2C(m\omega^2-k)\cos\theta}\frac{\omega_1^2-\omega^2+Ab_2^*}{\omega_1^2-\omega^2}=b_1^*R \quad (15a)$$

$$T_2^* = \frac{1}{\omega}\left\{(2n+1)\pi + a\tan\frac{2c\omega(m\omega^2-k)}{(m\omega^2-k)^2-(c\omega)^2}\right\}, \qquad (15b)$$

where $R = \frac{\omega_1^2-\omega^2+Ab_2^*}{\omega_1^2-\omega^2}$. In both Eqs. 13b and 15b, the period of successive passages of the tool T_1^* and T_2^* are the same. Comparing Eq. 13a to Eq. 15a, the difference is R, where $\omega_1 > \omega$ and $R > 1$ is produced due to the deflection of a workpiece. Hence, in terms of workpiece deflection, it can be concluded that a large deflection which corresponds to the large value of Ab_2^* results in a large allowable critical chip width.

When the workpiece is pressed by the tool, the workpiece will deflect along the direction of force and the real chip thickness will be changed. The value of R is also related to ω_1. When the deflections are assumed to be the same, the lower the natural frequency, the larger of the value R. Hence, the allowable critical chip width becomes larger.

4 Simulation results and discussion

The parameters of the tool and the workpiece used in simulation are listed in Table 1. From Fig. 3a , the length and radius of steel workpiece are 0.5 m and 0.06 m, respectively. The solid line represents the flexible case, while the dashed line represents the rigid case. The results show that there exists a larger critical chip width for each spindle speed in the deflection case. In Fig. 3b, the difference between these two cases is shown. Each lobe of Fig. 3b has a minimum value at the location closed to center point. Figure 3c shows the results of the critical chip width difference – the percentage difference between b_2^* and b_1^*. From the results in Fig. 3c, it can be found that the largest percentage of critical chip width difference is over 100%, and the smaller the value of n, the larger the percentage of critical chip width difference.

Figure 4 shows the results of steel workpiece with a length of less than 0.5 m with four different radius values. The lateral axis represents the spindle speed and the longitudinal axis represents the percentage of critical chip width difference. From the results in Fig. 4, the smaller the radius, the larger the percentage of critical chip width difference. This can be explained by the fact that the smaller the radius, the larger the deflection, which results in a larger critical chip width.

Figure 5 shows the results of steel workpiece with a radius of 0.06 m for two different values in length. From these results, it can be seen that the longer the length, the larger the percentage

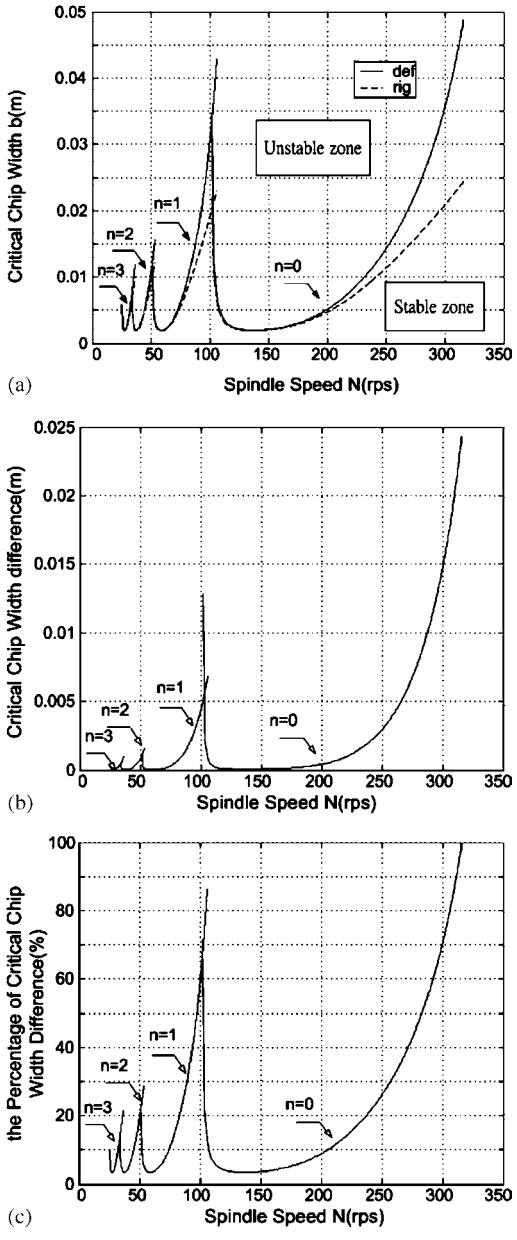

Fig. 3a–c. Comparative figure with and without deflection of a steel workpiece **a** The critical chip width with and without consideration of deflection of a steel workpiece **b** The difference of the critical chip width with and without consideration of deflection of a steel workpiece **c** The differential percentage of the critical chip width with and without consideration of deflection of a steel workpiece

Table 1. The parameters of tool and workpieces

Tool	m (kg)	c (kg/s)	k (N/m)	C (N/m^2)	θ (deg)
	50	2×10^3	2×10^7	2×10^9	70
Workpiece	steel	E_s(Gpa)	ρ_s(kg/m^3)	L (m)	r (m)
		180	7 600	0.5,0.25	0.035,0.0357,0.06, 0.07,0.08,0.10,0.14
	bronze	E_b	ρ_b	L (m)	r (m)
		100	8 600	0.5	0.07

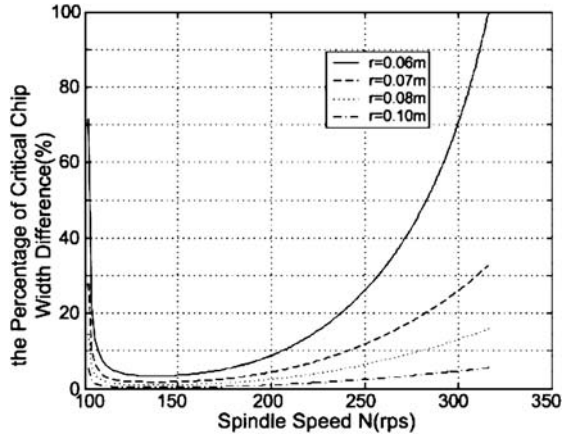

Fig. 4. Differential percentage of critical chip width for same length (0.5 m) and different radii of steel workpieces

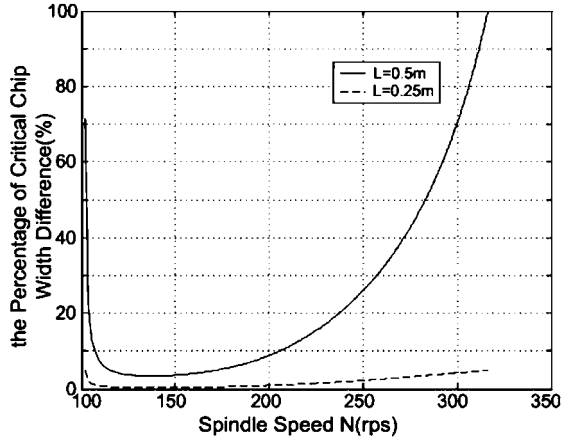

Fig. 5. Differential percentage of critical chip width for same radius and different length of steel workpieces

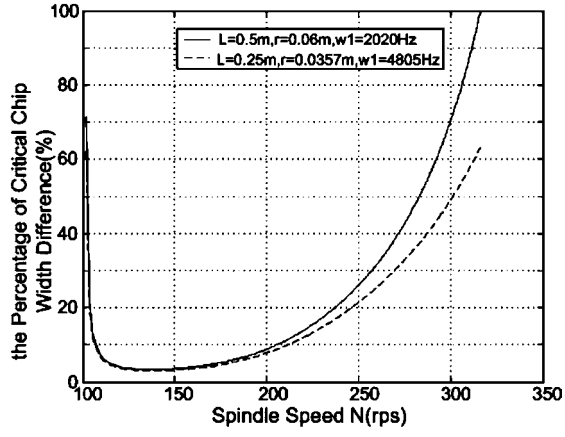

Fig. 6. Differential percentage of critical chip width for the same deflection of steel workpieces

of critical chip width difference. The reason is due to the fact that the longer the length, the larger the deflection, which results in the larger critical chip width.

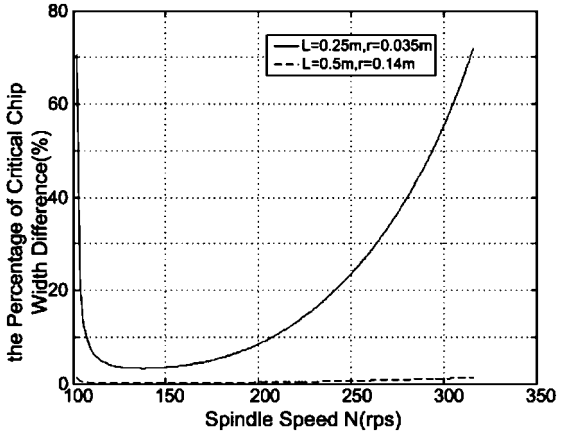

Fig. 7. Differential percentage of critical chip width for the same natural resonance frequency of steel workpieces

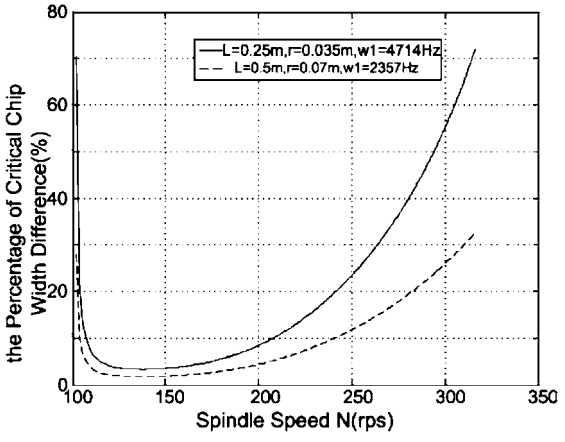

Fig. 8. Differential percentage of critical chip width for the same slenderness ratio of steel workpieces

Figure 6 shows the results of steel workpieces under the same deflection for two different workpiece conditions. The first has a length of 0.5 m, a radius of 0.06 m and a natural frequency 2020 Hz; the second one has a length of 0.25 m, a radius of 0.0357 m and a natural frequency of 4805 Hz. The results show that the smaller ω_1, the larger value of R. The value of R can be calculated from $R = \frac{\omega_1^2 - \omega^2 + Ab}{\omega_1^2 - \omega^2}$ and $R > 1$. Therefore, the critical chip width is larger for smaller radii and larger lengths. The simulation results are consistent with the theoretical analysis.

Figure 7 shows the results under the same natural frequency with two different steel workpieces conditions. The first has a length of 0.25 m and a radius of 0.035 m; the second has a length of 0.5 m and a radius of 0.14 m. Comparing the values of R, it can be concluded that the larger the deflection, the larger value of Ab, which corresponds to the larger critical chip width. The simulation results are also consistent with the theoretical analysis.

Figure 8 shows the results with the same slenderness ratio with two steel workpieces conditions. The first has a length of

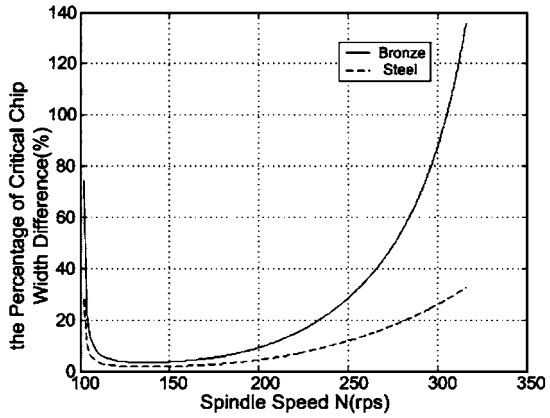

Fig. 9. Differential percentage of critical chip width for the same length and radius, different material

0.25 m and a radius of 0.035 m; the second has a length of 0.5 m and a radius of 0.07 m. Under these assumptions, the 0.25 m case has both a larger deflection and a larger critical chip width than the other case. In addition, the 0.5 m case has lower natural frequency and larger critical chip width than the other case. In comparing the allowable chip width in these two cases, only the numerical value of R is decisive. The results in Fig. 8 show that the 0.25 m case has a larger R than the 0.5 m case.

When considering the effect of different materials such as steel and bronze under the same lengths and radii, bronze has a larger deflection and a lower natural frequency than steel. Theoretically, the critical chip width of bronze should be larger than steel, which coincides with the simulation results shown in Fig. 9.

*Remark: the results shown in Figs. 4–9 are computed with $n = 0$.

5 Conclusion

In this study, we considered a flexible body workpiece that can be bent when a force is exerted on it. Such flexibility will affect the cutting force due to workpiece deflection and will result in a smaller real chip thickness and larger critical chip width. Under the same natural frequency, both the workpiece deflection and the critical chip width will become larger. Under the same workpiece deflection, the smaller the natural frequency, the larger the critical chip width.

For the case of a relatively slender workpiece being machined at a high spindle speed, the deformation will increase, having a great effect on the stable analysis. The method proposed in this article is helpful in solving such problems.

Nomenclature

b	chip width (m)
C	cutting force coefficient
c	equivalent damping (kg/s)
F	cutting force magnitude (N)
h	instantaneous chip thickness (m)
h_0	nominal chip thickness (m)
j	imaginary unit
k	equivalent stiffness (N/m)
m	equivalent mass (kg)
N	spindle speed (rps)
n	number of full waves
y	offset chip thickness (m)
θ	cutting force angle (deg)
T	the period of successive passages of the tool (s)
μ	overlapping factor
u	deflection (m)
$\phi, \phi_1 \ldots \phi_n$	eigen function
E	modulus of elasticity (Pa)
I	moment of inertia (m^4)
ρ	density (kg/m)
A_c	cross section area (m^2)
$A_1, \ldots, A_n$	coefficient of eigen function
$\omega_1, \ldots, \omega_n$	natural frequency of the workpiece (Hz)
L	length of workpiece (m)
$\alpha, \alpha_1, \ldots, \alpha_n$	eigen value
δ	impulse function

Acknowledgement The authors would like to thank the National Science Council, Taiwan, for the financial support under grant number NSC93-2622-E-269-014-CC3, and Professor Wang, J. J. Department of Mechanical Engineering National Cheng Kung University, Taiwan, for his generous advice at this research.

References

1. Tobias SA (1961) Machine tool vibration. Wiley, New York
2. Koenigs Berger F, Tlusty J (1971) Structure of machine tools. Pergamon Press, Oxford.
3. Merchant ME (1944) Basic mechanics of the metal-cutting process. Trans ASME J Appl Mech 11(3)A–168–A–175
4. Kegg RL (1965) Cutting dynamics in machine tool chatter. J Eng Ind 87(4):464–470
5. Merritt HE (1965) Theory of self excited machine tool chatter. J Eng Ind 87(4):447–454
6. King RI (1985) Handbook of high speed machining technology. Chapman and Hall, New York
7. Welbourn DB, Smith JD (1970) Machine tool dynamics – an introduction. Cambridge University Press, London.
8. Gradisek J, Govekar E, Grabec I (1996) A chaotic cutting process and determining optimal cutting parameter values using neural networks. Int J Mach Tools Manuf 36(10):1161–1172
9. Rao Balkrishua C, Shin Yung C (1999) A comprehensive dynamic cutting force model for chatter prediction in turning. Int J Mach Tools Manuf 39(10):1631–1654
10. Altintas Y, Budak E (1995) Analytical prediction of stability lobes in milling. Ann CIRP 44(1):357–362
11. Minis I, Yanushevsky T (1993) A new theoretical approach for the prediction of machine tool chatter in milling. Trans ASME J Eng Ind 115(1):1–8
12. Smith S, Tlusty J (1993) Efficient simulation programs for chatter in milling. Ann CIRP 42(1):463–466

13. Weck M, Altintas Y, Beer C (1994) CAD assisted chatter free NC tool path generation in milling. Int J Mach Tool Des Res 34(6):879–891
14. Tarng YS, Kao JY, Lee EC (2000) Chatter suppression in turning operations with a turned vibration absorber. J Mater Process Technol 105(1–2):55–60
15. Pitstra WC, Pieper JK (2000) Controller designs for constant cutting force turning machine control. ISA Trans 39(2):191–203
16. Soliman E, Ismail F (1997) Chatter suppression by adaptive speed modulation. Int J Mach Tools Manuf 37(3):355–369
17. Olgac N, Hosek M (1998) A new perspective and analysis for regeneration machine tool chatter. Int J Mach Tools Manuf 38(7):783–798
18. Meirovitch L (1967) Analytical methods in vibrations. Macmillan, New York
19. Rao SS (1985) Mechanical vibrations. Addison-Wesley, Boston